Pergamon

Geochimica et Cosmochimica Acta, Vol. 66, No. 9, pp. 1627–1640, 2002

0016-7037/02 $22.00 + .00

PII S0016-7037(01)00872-9

CO_2 solubility and speciation in intermediate (andesitic) melts: The role of H_2O and composition

P. L. KING[1,*,†] and J. R. HOLLOWAY[1,2]

Departments of [1]Geology and [3]Chemistry, Arizona State University, Tempe, AZ 85287 USA

(*Received October* 18, 2000; *accepted in revised form November* 7, 2001)

Abstract—We determined total CO_2 solubilities in andesite melts with a range of compositions. Melts were equilibrated with excess C-O(-H) fluid at 1 GPa and 1300°C then quenched to glasses. Samples were analyzed using an electron microprobe for major elements, ion microprobe for C-O-H volatiles, and Fourier transform infrared spectroscopy for molecular H_2O, OH^-, molecular CO_2, and CO_3^{2-}. CO_2 solubility was determined in hydrous andesite glasses and we found that H_2O content has a strong influence on C-O speciation and total CO_2 solubility. In anhydrous andesite melts with ~60 wt.% SiO_2, total CO_2 solubility is ~0.3 wt.% at 1300°C and 1 GPa and total CO_2 solubility increases by about 0.06 wt.% per wt.% of total H_2O. As total H_2O increases from ~0 to ~3.4 wt.%, molecular CO_2 decreases (from 0.07 ± 0.01 wt.% to ~0.01 wt.%) and CO_3^{2-} increases (from 0.24 ± 0.04 wt.% to 0.57 ± 0.09 wt.%). Molecular CO_2 increases as the calculated mole fraction of CO_2 in the fluid increases, showing Henrian behavior. In contrast, CO_3^{2-} decreases as the calculated mole fraction of CO_2 in the fluid increases, indicating that CO_3^{2-} solubility is strongly dependent on the availability of reactive oxygens in the melt. These findings have implications for CO_2 degassing. If substantial H_2O is present, total CO_2 solubility is higher and CO_2 will degas at relatively shallow levels compared to a drier melt. Total CO_2 solubility was also examined in andesitic glasses with additional Ca, K, or Mg and low H_2O contents (<1 wt.%). We found that total CO_2 solubility is negatively correlated with (Si + Al) cation mole fraction and positively correlated with cations with large Gibbs free energy of decarbonation or high charge-to-radius ratios (e.g., Ca). Combining our andesite data with data from the literature, we find that molecular CO_2 is more abundant in highly polymerized melts with high ionic porosities (>~48.3%), and low nonbridging oxygen/tetrahedral oxygen (<~0.3). Carbonate dominates most silicate melts and is most abundant in depolymerized melts with low ionic porosities, high nonbridging oxygen/tetrahedral oxygen (>~0.3), and abundant cations with large Gibbs free energy of decarbonation or high charge-to-radius ratio. In natural silicate melt, the oxygens in the carbonate are likely associated with tetrahedral and network-modifying cations (including Ca, H, or H-bonds) or a combinations of those cations. *Copyright © 2002 Elsevier Science Ltd*

1. INTRODUCTION

Water and carbon dioxide are the major volatile species in igneous rocks and they dominate the gas emitted from active andesitic volcanoes (Symonds et al., 1994). Relative to H_2O, CO_2 is less soluble in silicate melts, and as pressure decreases CO_2 is preferentially partitioned into a gaseous phase or low-density supercritical fluid. For this reason, CO_2 solubility models are needed to model volcanic degassing, bubble nucleation, and the formation of hydrothermal ore deposits.

CO_2 solubility data, expressed as molecular CO_2 ($CO_{2\ mol}$) + carbonate (CO_3^{2-}) recalculated as total ($CO_{2\ total}$), exist for a variety of natural and synthetic systems (Blank and Brooker, 1994; Dixon et al., 1995; Jakobsson, 1997; Jendrzejewski et al., 1997; Brooker et al., 1999; Morizet et al., 2001). Despite these studies, general $CO_{2\ total}$ solubility models for mafic through silicic compositions have large errors (Spera and Bergman, 1980; Papale, 1999; Brooker et al., 2001a). The errors arise from CO_2 measurements using β-track autoradiography techniques (inaccuracies of 10–50%; Tingle and Aines, 1988), or bulk techniques that overestimate $CO_{2\ total}$ content (King et al., 2002), particularly if CO is present. The only $CO_{2\ total}$ solubility model that exclusively uses modern microanalytical techniques, and thus the only model that accurately represents the data, is restricted to mafic compositions (Dixon, 1997).

General trends in $CO_{2\ total}$ solubility and speciation have been summarized elsewhere (Blank and Brooker, 1994; Holloway and Blank, 1994; Brooker et al., 2001a). Although intermediate rocks are volumetrically important in subduction zones, there are few studies of $CO_{2\ total}$ solubility in these compositions (Mysen et al., 1975; Shilobreyeva and Kadik, 1990; Brooker et al., 2001a; Morizet et al., 2001). In this paper, we examine $CO_{2\ total}$ solubility in intermediate rocks with varying Ca, K, and Mg contents because a range of intermediate compositions exists in nature (e.g., low-K tholeiitic through high-K alkali andesites; Gill, 1981).

Because the amount of H_2O in magmas generally exceeds the amount of CO_2, the effect of dissolved H_2O on CO_2 solubility is likely to be important, whereas the effect of dissolved CO_2 on H_2O is negligible. We also examine how $CO_{2\ total}$ solubility is affected by the total H_2O content of the melt (H_2O_{total}), which is a reflection of H_2O activity (a_{H_2O}) in the system. This is a topic of interest because there is a dispute as to whether changes in a_{H_2O} affect $CO_{2\ total}$ solubility, and therefore whether $CO_{2\ total}$ solubility is proportional to carbon dioxide activity (a_{CO_2}) and thus follows Henry's Law. Experi-

* Author to whom correspondence should be addressed (penny.king@uwo.ca).
[2]*Present address:* Department of Earth Sciences, University Western Ontario, London, ON N6A 5B7 Canada.

Table 1. Representative andesites and MHA-comp experiments.

Andesite	MHA	MHA	Med K	High K	Med Ca	High Ca	High Mg
Experiment	Juli9	MHA23	MHA52	MHA46	MHA47	MHA50	MHA51
OA/OAD added wt.%[a]	4.54	1.05	6.03	4.73	5.45	5.32	5.37
Cation source added wt.%	0.0	0.0	1.02 K_2CO_3	2.04 K_2CO_3	1.51 $CaCO_3$	5.5 $CaCO_3$	0.92 MgO
Capsule (in/out)	AuPd/Pt	Fe-Pt	AuPd/Pt	AuPd/Pt	AuPd/Pt	AuPd/Pt	AuPd/Pt
Outer capsule powder	QtzAbHm	none	QtzAb	QtzAbHm	QtzAbHm	QtzAb	QtzAb
Fluid-phase solute	none	none	little	little	little	little	little
Melt ΔNNO, initial	—	1.02	1.17	1.01	1.05	1.03	1.23
Eprobe analyses (wt.%)							
No.	7	5	4	4	4	4	4
SiO_2	59.98	59.57	61.17	57.86	58.90	59.35	61.21
TiO_2	0.86	0.92	0.88	0.90	0.91	0.87	0.89
Al_2O_3	18.34	18.07	18.62	18.54	18.60	17.81	18.57
Fe_2O_3[b]	5.37	5.24	5.76	4.57	4.69	3.85	3.85
FeO[b]	0.61	0.62	0.68	0.54	0.55	0.48	0.45
FeO_{total}	4.82	4.69	5.15	4.08	4.19	3.41	3.44
MnO	0.06	0.08	0.07	0.08	0.08	0.10	0.07
MgO	2.57	2.66	2.79	2.68	2.73	2.69	3.64
CaO	5.71	6.05	5.88	5.81	6.76	8.33	5.84
Na_2O	4.56	4.83	4.57	4.36	4.46	4.42	4.60
K_2O	0.91	0.93	1.52	2.22	0.90	0.90	0.96
P_2O_5	0.36	0.20	0.25	0.22	0.26	0.20	0.24
Total	98.79	98.64	101.57	97.29	98.34	98.56	99.90
No. SIMS analyses	2	4	3	3	3	3	3
H_2O SIMS (wt. %)[c]	0 (0.30)	0.76 (0.10)	0.28 (0.05)	0.46 (0.09)	0.34 (0.03)	0.53 (0.04)	0.60 (0.08)
No. FTIR analyses[c]	5	6	4	7	4	5	4
OH^- FTIR (wt. %)	0.14 (0.08)	0.31 (0.02)	0.33 (0.02)	0.66 (0.07)	0.35 (0.01)	0.65 (0.04)	0.70 (0.02)
ε_{1550} ($Lmol^{-1}cm^{-1}$)	271	271	276	278	286	298	276
$CO_{2\ total}$ FTIR (wt. %)	0.31 (0.04)	0.42 (0.04)	0.40 (0.04)	0.42 (0.05)	0.39 (0.04)	0.52 (0.05)	0.41 (0.05)
$CO_{2\ mol}$ FTIR (wt. %)	0.07 (0.01)	0.08 (0.01)	0.07 (0.01)	0.06 (0.01)	0.06 (0.01)	0.03 (0.004)	0.05 (0.01)
CO_3^{2-} FTIR (wt.%)	0.24 (0.03)	0.34 (0.03)	0.33 (0.03)	0.36 (0.04)	0.33 (0.03)	0.49 (0.05)	0.36 (0.04)
$CO_{2\ mol}/CO_3^{2-}$	0.29	0.24	0.21	0.17	0.18	0.06	0.14
Mole fraction in melt							
X^m_{OH-}	0.28	0.61	0.66	1.30	0.69	1.27	1.35
$X^m_{CO_{2\ mol}}$*1000	0.53	0.59	0.57	0.44	0.48	0.20	0.38
$X^m_{CO_3^{2-}}$*100	0.18	0.26	0.26	0.28	0.25	0.37	0.27

[a] OA was added to all samples except OAD was added to MHA23 and Juli9. Samples were oversaturated in total CO_2 based on solubilities in other silicate melts. H_2O was minimized in the starting materials.

[b] Fe_2O_3 and FeO calculated at NNO following Kress and Carmichael (1988).

[c] SIMS errors calculated using the larger value of a) 1σ of the average of several analyses, or b) 1σ of the background analyses. FTIR errors are calculated based on 1σ of the average of several analyses; note that this is a little smaller than the systematic error on the extinction coefficient as described in the text.

ments on various compositions at high pressure have shown that $CO_{2\ total}$ solubility is either enhanced by higher a_{H_2O} (Holloway and Lewis, 1974; Mysen et al., 1976; Eggler and Rosenhauer, 1978; Eggler and Kadik, 1979; Holloway, 1981); or unaffected by a_{CO_2} (Jakobsson, 1997). In both cases, Henry's Law does not readily describe $CO_{2\ total}$ solubility. In contrast, low pressure experiments on basaltic and rhyolitic melts showed that $CO_{2\ total}$ solubility is a simple function of a_{CO_2} (Henry's Law is obeyed; Blank et al., 1993; Dixon et al., 1995).

We pay particular attention to the C-O speciation in evaluating $CO_{2\ total}$ solubility mechanisms because intermediate glasses contain both CO_3^{2-} and $CO_{2\ mol}$ species, in contrast to mafic glasses that contain only CO_3^{2-} and felsic glasses that contain only $CO_{2\ mol}$. Furthermore, we use the splitting of the IR-active CO_3^{2-} ν_3 doublet ($\Delta\nu_3$) as a tool to examine the $CO_{2\ total}$ solubility mechanisms. Typical silicate melts have $\Delta\nu_3$ values of ~70 to 100 cm^{-1} which are thought to result from distortion of the CO_3^{2-} from trigonal planar symmetry (D_{3h}, $\Delta\nu_3 < 10$ cm^{-1} in "symmetrical" CO_3^{2-}; Brooker et al., 2001b). In andesites, the $\Delta\nu_3$ values are thought to result from interactions between CO_3^{2-} and the silicate network tetrahedral cations (T cations, such as Si^{4+}, Al^{3+} Fe^{3+}), or network-modifying cations (M^{n+}, such as Ca^{2+}, Mg^{2+}, or Fe^{2+}), or the presence of nonequivalent sites that lower the symmetry (Taylor, 1990; Brooker et al., 2001b).

2. EXPERIMENTAL METHODS

We conducted two sets of experiments using natural andesite from Mt. Hood, Oregon, USA (MHA) because it has a composition that is typical of calc-alkaline rocks (Table 1; cf. the medium K-andesite composition of Gill, 1981). The first set examined the effects of changing H_2O content on $CO_{2\ total}$ solubility (MHA-H_2O experiments).

The second set examined the effects of changing Ca, K, and Mg contents (MHA-comp experiments).

Experimental methods were similar to those described in King et al. (2002), and we use some of those results in this study. For experiments under oxidizing conditions (magnetite:hematite buffer; MH), the starting material was preequilibrated under a stream of CO_2 for 24 h. For the MHA-comp experiments, the natural andesite was mixed with reagent-grade carbonate ($CaCO_3$ or K_2CO_3) or oxide (MgO). The compositions produced were all metaluminous and similar to natural andesites (Table 1).

Experiments were performed in a 12.7-mm (0.5“) non-end-loaded piston-cylinder apparatus following techniques described in detail in King et al. (2002). Run conditions were 1300°C and 1 GPa. The samples were contained in either 5-mm-diameter Fe-doped Pt capsules which held 115 to 200 mg of sample, or 3-mm-diameter, 6-mm-long $Au_{75}Pd_{25}$ inner capsules that held ~40 to 50 mg of sample. The Fe-doped Pt capsules were prepared in contact with molten Fe-rich trachyte in a one-atmosphere gas-mixing furnace then cleaned in HF. The $Au_{75}Pd_{25}$ alloy results in less Fe-“loss” from the melt to the capsule than other high-temperature capsule materials such as Pt (Kawamoto and Hirose, 1994), and we found that it is moderately permeable to H_2 (King et al., 2000). Samples were added to capsules with the volatile source first, followed by the andesite powder ($\leq$50 μm grain size). For the MHA-H_2O experiments, the volatile sources were distilled, deionized H_2O and oxalic acid dihydrate ($H_2C_2O_4 \cdot 2H_2O$; OAD) following Holloway et al. (1968). For the MHA-comp experiments, we tried to minimize H content and the C source was either oxalic acid dihydrate or oxalic acid ($H_2C_2O_4$; OA), and in some cases carbonate (Table 1). The volatile sources were added such that all experiments were saturated in total CO_2 content, based on solubilities for other silicate melts (Holloway and Blank, 1994, Tables 1 and 2). After loading, the capsules were arc-welded shut while wrapped in a water-soaked and frozen tissue to minimize volatile loss. To test for leaks, capsules were submerged in hot mineral oil (>250°C) for at least 20 s.

For the MHA-comp experiments, the $Au_{75}Pd_{25}$ inner capsules were surrounded by a powder enclosed in an outer Pt capsule. The compositions of the powders used in the outer capsule are listed in Tables 1 and 2. Some outer capsules contained quartz-albite (quartz:albite = 10:3 mol, eutectic = 3:4 mol at 675°C and 1 GPa; Luth et al., 1964) to produce a felsic melt with high H_2O solubility that would reduce the H content of the inner andesite sample. This viscous melt also captured the quenched fluid phase as inclusions that could be analyzed with spectroscopic methods. Some outer capsules contained pure magnetite or hematite in an attempt to monitor oxygen fugacity (f_{O_2}) using the Fe content of the Pt; however, this method was unsuccessful (King, 1999).

3. ANALYTICAL TECHNIQUES

Electron microprobe, ion microprobe (secondary-ion mass spectrometry [SIMS]), and Fourier transform infrared (FTIR) spectroscopy analyses of the glasses were performed (techniques in King et al., 2002). The FeO content of the starting material was obtained via titration (Activation Laboratories Ltd., Ontario, Canada; Table 1).

Volatile speciation was determined using FTIR spectra obtained at the United States Geological Survey (USGS), Menlo Park, California (Fig. 1). Spectra were collected using a Nicolet Magna 750 FTIR spectrometer with microscope and a KBr beam splitter and MCT-A detector. Each spectrum was obtained with 4 cm^{-1} resolution and 1000 to 1500 scans, with the background analyzed periodically. The entire system was continuously purged with dry air and spectra were measured on at least four locations within a sample. Each sample was doubly polished and the thickness measured using two different vertically mounted Miyutomo micrometers with estimated errors of ± 2 μm.

To convert absorbance peaks to concentrations the peak heights were measured after subtracting curved baselines (methods in King et al., 2002). The Beer-Lambert law was then applied:

$$c = \frac{MW\ A}{d\ \rho\ \varepsilon} \quad (1)$$

where c is the concentration, MW is the molecular weight of the volatile species, A is the absorbance, d is the sample thickness, ε is the extinction coefficient, and ρ is the glass density (calculated following King et al., 2002). The H-O species concentrations were calculated using the extinction coefficients for molecular H_2O (H_2O_{mol}) and hydroxyl (OH^-) of $\varepsilon_{5200} = 1.08 \pm 0.11$ $Lmol^{-1}cm^{-1}$ and $\varepsilon_{4500} = 1.15 \pm 0.11$ $Lmol^{-1}cm^{-1}$ respectively (King et al., 2002). For CO_3^{2-} concentrations, the CO_3^{2-} extinction coefficient (ε_{1550}) was calculated using an empirical relationship that accounts for changes in ε_{1550} as a function of Na and Ca content: 412 - 232 * {Na/(Na + Ca)} (Dixon and Pan, 1995; King et al., 2002). We estimate a systematic error of ~10% for the MHA-H_2O and MHA-comp experiments and assume that this equation is valid for all MHA-comp experiments because the position of the CO_3^{2-} doublet is near constant for all MHA-comp experiments, except those with variable Ca contents which are accounted for in the equation (cf. Brooker et al., 2001b). For $CO_{2\ mol}$, we used an extinction coefficient of 945 $Lmol^{-1}cm^{-1}$ which has a systematic error of ~16% (King et al., 2002). The C-H-O species present in the glasses likely represent the species present in the high-temperature melt, based on high-temperature FTIR studies of H-O-rhyolite liquids (Withers et al., 1999; Nowack and Behrens, 2001) and estimates of C-O speciation above the glass transition temperature in Na-Al-Si-O glasses (Brooker et al., 1999).

4. OXYGEN FUGACITY

Relatively f_{O_2} conditions could lower $CO_{2\ total}$ solubility and produce a CO-rich fluid phase (Pawley et al., 1992). In these experiments, the melt f_{O_2} ($f_{O_2}^{melt}$) was controlled by the starting material composition and the furnace assembly (Brooker et al., 1998). If $f_{O_2}^{melt}$ is calculated using the starting compositions (following Pan et al., 1991), we obtain a maximum value of one log unit above the nickel-nickel oxide buffer (NNO + 1; Table 2). However, this method assumes that $f_{O_2}^{melt}$ equals fluid f_{O_2} ($f_{O_2}^{fl}$) and that the C-O species in the fluid are in equilibrium with the Fe-O species in the melt following: $CO_2^{fl} + 2FeO^m = CO^{fl} + Fe_2O_3^m$. The assumption of equilibrium is questionable because the run durations were short and it is likely that the experiments became more reducing as H_2 or C diffused into samples with a low initial H or C content relative to the furnace assembly (King et al., 2002). The minimum $f_{O_2}^{melt}$ value is poorly defined, but is more oxidizing than NNO-2 because graphite and CO were not identified in the andesite glasses by FTIR or Raman (King, 1999). Thus, we discuss the experiments in the context of $f_{O_2}^{melt}$ values of NNO, although the range is likely NNO + 1 to NNO − 1. In this range, the mole fraction of CO_2 in the fluid ($X_{CO_2}^{fl}$) dominates relative to the mole fraction of CO in the fluid (X_{CO}^{fl}), with calculated $X_{CO_2}^{fl}/(X_{CO_2}^{fl} + X_{CO}^{fl}) > 0.9$, and there is negligible calculated CH_4.

5. RESULTS

Features and chemical compositions of experiments with a C-O-H-fluid phase are listed in Tables 1 and 2. Experimental products were clear, brown glasses with bubbles and the glasses had no surface coatings or crystals. Glass compositions, measured by electron probe microanalysis (Tables 1 and 2), did not vary greatly within each sample and FeO was depleted up to 1 wt.% (absolute) relative to the starting material. The only C-O-H species in the glasses, based on FTIR and Raman analysis (King, 1999), are $CO_{2\ mol}$, CO_3^{2-}, H_2O, and OH^- with no CO or CH_4. Experiments with a large initial excess of initial CO_2 contained a quenched fluid-phase solute (Tables 1 and 2).

The MHA-H_2O experiments have $CO_{2\ total}$ contents measured by FTIR that increase from 0.31 to 0.58 wt.% as H_2O contents increase from 0 to 3.39 wt.% (Fig. 2A, Table 2). This represents an increase in $CO_{2\ total}$ solubility of ~0.06 wt.% per wt.% of H_2O (Fig. 2A). As H_2O_{total} content increases, CO_3^{2-} increases, $CO_{2\ mol}$ content decreases slightly or remains constant (Table 2 and King et al., 2002). Despite the correlation between C-O speciation and H_2O_{total}, there is no obvious correlation between C-O speciation and H-O speciation (Fig. 2B,C). Instead, the H-O species follow trends similar to the trends for H-O species in

Table 2. MHA-H_2O experiments.

Sample	Juli9	MHA23	MHA12	MHA6	MHA44	Juli12
Run duration (min)	120	120	120	120	20	120
Total CO_2 % initial[a]	3.13	0.72	5.24	6.74	0.72	6.57
Total H_2O% initial	0[b]	0.30	2.20	4.77	3.69	5.26
Bubbles	no	few	no	no	few	yes
Fluid-phase solute	no	no	no	yes	little	yes
Capsule (in/out)	AuPd/Pt	Fe-Pt	AuPd/Pt	AuPd/Pt	Fe-Pt	AuPd/Pt
Outer capsule material	QtzAbHm	none	Mt-Hm=1:30	Mt-Hm=1:30	none	Basalt
Eprobe analyses (wt.%), No.	5	5	5	10	6	7
SiO_2	59.98	59.57	57.25	58.79	58.10	56.80
TiO_2	0.86	0.92	0.89	0.85	0.85	0.89
Al_2O_3	18.34	18.07	17.42	17.31	18.35	17.42
FeO_{total}	5.37	5.25	5.67	5.40	5.36	5.67
MnO	0.06	0.08	0.07	0.09	0.09	0.11
MgO	2.57	2.66	3.64	2.54	2.59	2.86
CaO	5.71	6.05	5.84	5.70	5.80	5.75
Na_2O	4.56	4.83	4.60	4.23	4.34	4.70
K_2O	0.91	0.93	0.96	0.90	0.86	0.91
P_2O_5	0.36	0.20	0.24	0.28	0.24	0.24
F	0.12	0.09	n.d.	0.12	n.d.	0.08
Total	98.84	98.67	98.10	96.21	96.58	95.44
Fe_2O_3/FeO calc. based on starting composition						
Fe_2O_3	1.60	1.63	1.63	1.64	1.63	1.72
FeO	3.82	3.90	3.90	3.93	3.89	4.12
ΔNNO initial	1.02	~1	1.25	1.35	1.12	1.25
Volatiles in glasses[c]						
H_2O technique, no. analyses	SIMS, 2	Manom, 1	SIMS, 4	SIMS, 4	SIMS, 7	SIMS, 2
H_2O_{total} (wt.%)	0 (0.30)	0.76 (0.10)	1.34 (0.82)	2.62 (0.19)	3.34 (0.37)	3.39 (0.35)
a_{H_2O} (melt)	0	0.02	0.12	0.29	0.26	0.33
FTIR analyses, no. analyses	5	6	3	3	7	3
$CO_{2\ total}$ (wt.%)	0.31 (0.04)	0.42 (0.04)	0.39 (0.07)	0.43 (0.05)	0.49 (0.05)	0.58 (0.06)
$CO_{2\ mol}$ (wt. % ± 10%)	0.07 (0.01)	0.08 (0.01)	0.06 (0.01)	0.03 (0.01)	0.01 (0.002)	0.01 (0.001)
CO_3^{2-} (wt.% ± 16%)	0.24 (0.03)	0.34 (0.03)	0.33 (0.06)	0.40 (0.04)	0.48 (0.05)	0.58 (0.06)
$CO_3^{2-}/CO_{2\ mol}$	0.29	0.24	0.18	0.08	0.02	0.02
Max. $\Delta\nu_3$(cm^{-1})	120	112	103	97	91	90
H_2O_{mol} (wt.%)	n.d.	n.d.	n.d.	1.57 (0.12)	1.97 (0.18)	2.20 (0.28)
OH^- FTIR (wt.%)	0.14 (0.08)	0.31 (0.02)	1.08 (0.23)	1.38 (0.05)	1.47 (0.07)	1.32 (0.11)
H_2O_{total} 3550 cm^{-1} FTIR (wt.%)	0.27 (0.10)	0.47 (0.10)	1.86 (0.37)	n.d.	3.97 (0.40)	n.d.
H_2O_{total} max error (wt.%)[d]	0.30	0.31	0.52	0.19	0.63	0.35
Volatiles in fluid						
$X^{fl}_{H_2O}$	0	no fluid	0.30	0.45	0.79	0.43
$X^{fl}_{CO_2}$ NNO	0.97		0.68	0.53	0.20	0.55
X^{fl}_{CO} NNO	0.03		0.02	0.02	0.01	0.02
Density[e]	2542 ± 43	2538 ± 49	2581 ± 31	2511 ± 5	2517 ± 12	2522 ± 1

[a] The initial CO_2 content of the starting material was 0.03 wt.%.
[b] H_2O lost from capsule during weld.
[c] Manom = manometry analyses. The a_{H_2O} calculations were made following Burnham (1979). n.d. = not determined. Errors determined as described in Table 1.
[d] Maximum error in the H_2O_{total} contents derived by examining the difference between FTIR and SIMS analyses.
[e] Density is calculated as described by King et al. (2002).

C-free andesites (Mandeville et al., 2001) and (C-)O-H bearing midocean ridge basalt (MORB) (Dixon et al., 1995).

Carbonate peak splitting ($\Delta\nu_3$, cm^{-1}) also varies as a function of H_2O_{total} in the MHA-H_2O experiments (Table 2, Fig. 1B, and King et al., 2002). As H_2O_{total} content increases, $\Delta\nu_3$ decreases, which indicates that the CO_3^{2-} bonding environment is more symmetrical (Taylor, 1990; Jakobsson, 1997).

Because H_2O enhances $CO_{2\ total}$ solubility, the MHA-comp experiments were restricted to having less than 1 wt.% H_2O so that the effect of major oxides on melt composition could be assessed independently (Table 1). In these experiments, CO_2 was present in excess, and $CO_{2\ total}$ solubility varies from 0.31 to 0.52 wt.% (Table 3). The sample with the most $CO_{2\ total}$ (MHA50) has low (Si + Al) mole fraction and the highest Ca mole fraction. It is unlikely that MHA50 has high $CO_{2\ total}$ content due to its H_2O (0.53 wt.%), because other samples with higher H_2O (MHA51 with H_2O = 0.60 wt.% and MHA23 with H_2O = 0.76 wt.%), have significantly lower $CO_{2\ total}$ content and different $CO_{2\ mol}/CO_3^{2-}$ (Table 1). Andesite samples with higher Ca have lower $\Delta\nu_3$, even when the effect of H_2O_{total} is taken into account (Table 3), indicating that the CO_3^{2-} bonding environment is more symmetrical.

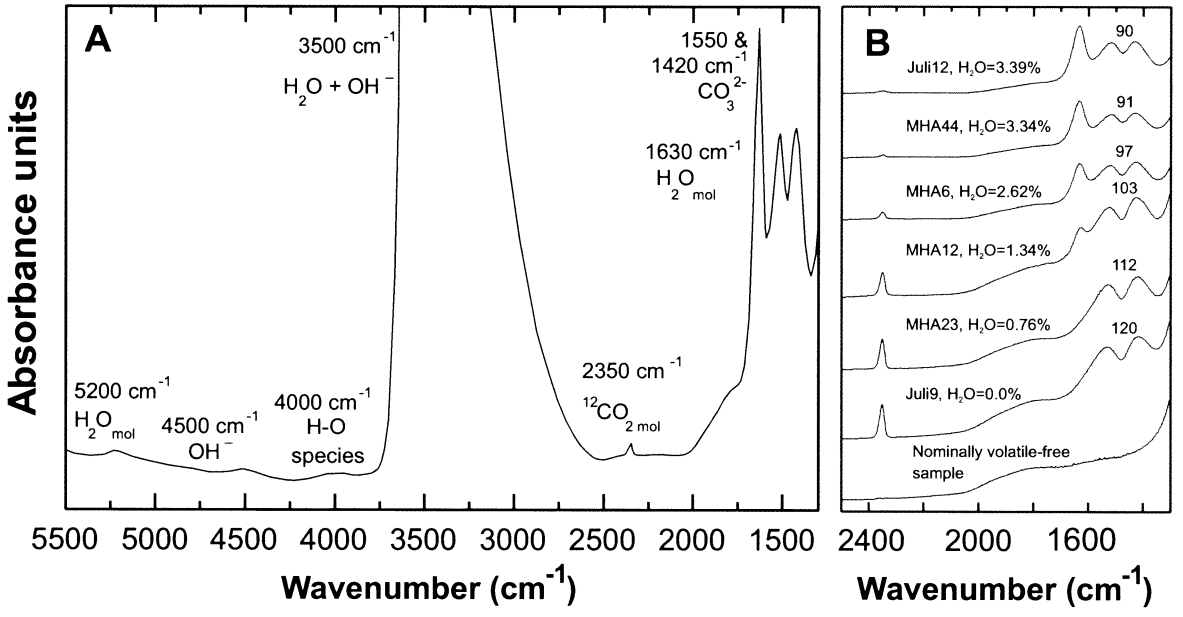

Fig. 1. (A) Typical FTIR spectrum showing the C-O-H species analyzed. (B) Spectra for the MHA-H_2O experiments illustrating the changes in the $CO_{2\ mol}$, CO_3^{2-}, and H_2O_{mol} peaks with increasing H_2O_{total} (%). The spectra have not been normalized to sample thickness and have been chosen to best illustrate the changes in the peaks.

6. DISCUSSION

Existing models for $CO_{2\ total}$ solubility propose two end-member reactions for CO_2 dissolution into a melt (summarized in Holloway and Blank, 1994):

$$CO_2^{fl} = CO_{2\,mol}^{m} \quad (2)$$

$$CO_{2\,mol}^{m} + O_r^{2-m} = CO_3^{2-m} \quad (3)$$

Here, O_r^{2-m}, the reactive oxygen in the melt, could include bridging oxygen, nonbridging oxygen, or "free" oxygen. Because the melts contain both CO_3^{2-} and $CO_{2\ mol}$ it is necessary to examine the solubility of each species to determine the roles of different parameters on $CO_{2\ total}$ solubility.

6.1. Effect of the Fluid Speciation on $CO_{2\ total}$ and H_2O_{total} Solubility

To examine how the fluid phase affects melt volatiles, we first calculated the mole fraction of C-O species in the melt ($X^m_{species}$) and the mole fraction of the C-O species in the fluid ($X^{fl}_{species}$). To calculate $X^m_{species}$, we used the equation: $X^m_{species}$ = {(mole of species)/[(100 − mole of H_2O_{total})/one-oxygen mole + mole of H_2O_{total} + mole of $CO_{2\ total}$]} (Blank et al., 1993; Dixon et al., 1995), where the one-oxygen mole for the MHA andesites is ~34 g, dependent on composition. To calculate $X^{fl}_{species}$, we first calculated the final ($X^{fl}_{CO_2} + X^{fl}_{CO}$) and $X^{fl}_{H_2O}$ as {amount of initial volatile vapor + amount of initial dissolved volatile − amount of final dissolved volatile}, assuming that $X^{fl}_{CO_2} + X^{fl}_{CO} + X^{fl}_{H_2O} = 1$, that the system was open to H_2, and that OA and OAD stoichiometrically form CO_2, H_2, and H_2O as shown by Holloway et al. (1968) at lower P and T. Once $X^{fl}_{CO_2} + X^{fl}_{CO}$ was known, $X^{fl}_{CO_2}$ and X^{fl}_{CO} were calculated at $f^{fl}_{O_2}$ = NNO (Table 2) using JANAF tables and fugacity coefficients from Saxena and Fei (1987). This method of calculating fluid species was chosen because it most closely fits experimental measurements (Frost and Wood, 1995).

$CO_{2\ total}$ solubility, expressed as the total mole fraction of CO_2 in the melt ($X^m_{CO_3^{2-}} + X^m_{CO_{2\ mol}}$), decreases with increasing $X^{fl}_{CO_2}$ (Table 2), which approximates a_{CO_2} in the melt ($a^m_{CO_2}$). The non-Henrian behavior is also observed for CO_3^{2-}, which is the dominant C-O species in andesitic melts (Fig. 3). We postulate that CO_3^{2-} is incorporated in the melt as a function of the availability of O_r^{2-m} (reaction 3), rather than the composition of the fluid phase (reactions 2 and 3). Deviations from Henrian behavior were reported for CO_3^{2-} solubility in icelandites at high pressure where $CO_{2\ total}$ remains constant with increasing CO_2 fugacity (Jakobsson, 1997), possibly because that melt was C-saturated for the range of CO_2 fugacities investigated. At low pressures, $CO_{2\ total}$ and CO_3^{2-} solubility are linearly dependent on $X^{fl}_{CO_2}$ in basalts (Dixon et al. 1995), possibly because the fugacity of CO_2 in the fluid is lower.

In contrast, $CO_{2\ mol}$ solubility is a near-linear function of $X^{fl}_{CO_2}$ (Fig. 3), thus near-Henrian behavior is observed. Molecular CO_2 in rhyolitic melts shows near-linear behavior at low pressure, but $CO_{2\ mol}$ solubility deviates from linearity to lower values at higher pressure and high $X^{fl}_{CO_2}$ (Tamic et al., 2001). Similar deviations from linearity would be expected for andesites also at high pressure and high $X^{fl}_{CO_2}$, but it may not be possible to distinguish these deviations because $CO_{2\ mol}$ solubility is so low that deviations are likely to be close to the errors of the analytical techniques.

Our experiments were not specifically designed to investigate the relationship between H_2O solubility and the mole fraction of H_2O in the fluid ($X^{fl}_{H_2O}$). However, a positive correlation is observed (Table 2), similar to the findings of other authors (Blank et al., 1993; Tamic et al., 2001).

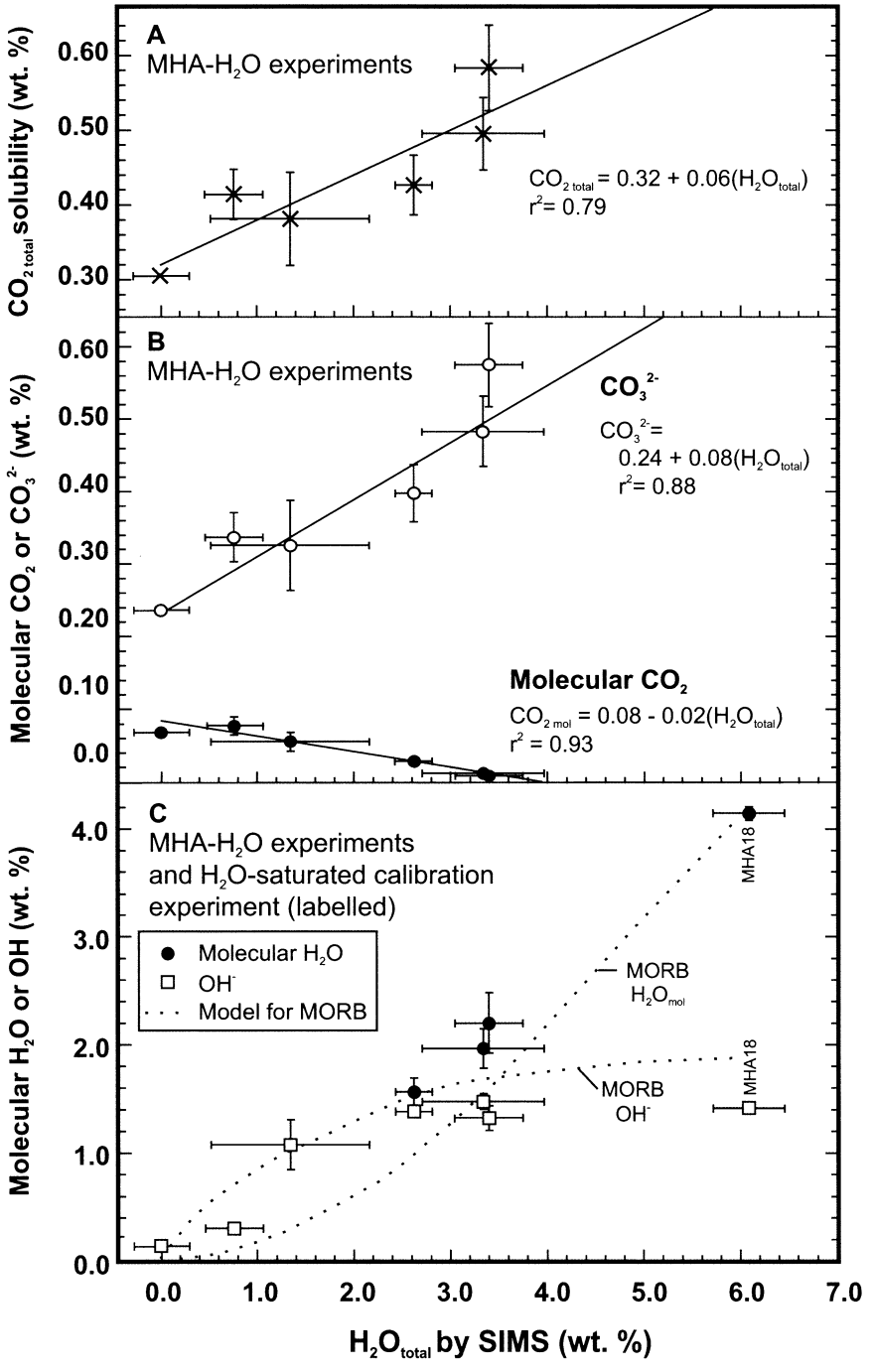

Fig. 2. (A) $CO_{2\ total}$ solubility determined by FTIR versus H_2O_{total} determined by SIMS and manometry for MHA-H_2O samples (C-saturated). (B) CO_3^{2-} and $CO_{2\ mol}$ versus H_2O_{total} for the MHA-H_2O samples. (C) OH^- and H_2O_{mol} versus H_2O_{total} for the MHA-H_2O samples and MHA18 from King et al. (2002). The MORB model lines for H_2O_{mol} and OH^- versus H_2O_{total} are after Dixon et al. (1995), as discussed in the text. The errors reported in all of the tables and figures for the FTIR analyses are one standard deviation of the average of several analyses; note that the systematic error described in the text is a little larger. The errors reported for the H_2O_{total} analyses are the largest value that results from either a) variation in the background H content for SIMS analyses, or; b) one standard deviation of the average of several SIMS analyses, or; c) the deviation of the SIMS analyses from the FTIR analyses.

6.2. Effect of H_2O on C-O Speciation and $CO_{2\ total}$ Solubility

As indicated above, H_2O_{total} content affects $CO_{2\ total}$, CO_3^{2-}, and $CO_{2\ mol}$ solubility, but there is no obvious relationship to H-O speciation (Fig. 2A–C). Also, FTIR CO_3^{2-} doublet peak $\Delta\nu_3$ for the MHA-H_2O experiments decreases as a function of H_2O_{total} (King et al., 2002) indicating increased symmetry in the CO_3^{2-} site.

Table 3. CO_2 solubility and compositional parameters for literature samples and andesites.

Composition	Andesites							Rhyolite	Albite	Icelandite	Tholeiite	Basanite	Leucitite
Sample	Juli9	MHA23	MHA52	MHA46	MHA47	MHA50	MHA51						
Reference	MHA	MHA	Med K	High K	Med Ca	High Ca	High Mg	Blank et al. 1993	Stolper et al. 1987	Jakobsson, 1997	Pan et al. 1991	Holloway and Blank, 1994	Thibault and Holloway, 1994
Sample prep.[a]	Piston-cylinder (P.C.), NNO-1 < fO_2 < NNO + 1							C. seal, NNO + 1	P.C.	P.C., 1400°C	P.C. NNO−0.5	P.C.	P.C. ~NNO + 1
C-O species solubility (wt.%)													
$CO_{2\ total}$	0.31 (0.04)	0.42 (0.04)	0.40 (0.04)	0.42 (0.05)	0.39 (0.04)	0.52 (0.05)	0.41 (0.05)	0.34	0.50	max. 1.03	1.27	1.20	2.85
$CO_{2\ mol}$	0.07 (0.01)	0.08 (0.01)	0.07 (0.01)	0.06 (0.01)	0.06 (0.01)	0.03 (0.004)	0.05 (0.01)	0.34	0.45	0.00	0.00	0.00	0.00
CO_3^{2-}	0.24 (0.03)	0.34 (0.03)	0.33 (0.03)	0.36 (0.04)	0.33 (0.03)	0.49 (0.05)	0.36 (0.04)	0.00	0.05	1.03	1.27	1.20	2.85
$CO_{2\ mol}/CO_3^{2-}$	0.29	0.24	0.21	0.17	0.18	0.06	0.14	-	9.00	0.00	0.00	0.00	0.00
C-O species mole fraction in the melt													
$X^m_{CO_{2\ total}}$ *100	0.23	0.32	0.32	0.32	0.30	0.39	0.31	0.26	0.39	0.80	0.99	0.93	2.22
$X^m_{CO_3^{2-}}$ *100	0.18	0.26	0.26	0.28	0.25	0.37	0.27	0.00	0.04	0.80	0.99	0.93	2.22
$X^m_{CO_{2\ mol}}$ *100	0.53	0.59	0.57	0.44	0.48	0.20	0.38	2.62	3.49	0.00	0.00	0.00	0.00
Max. $\Delta\nu_3$ (cm^{-1})	120	112	108	112	106	93	105	n/a[c]	235	100	100	109	85
Cation fraction													
Si	0.560	0.556	0.556	0.546	0.551	0.554	0.561	0.724	0.612	0.519	0.425	0.456	0.405
Ti	0.006	0.006	0.006	0.006	0.006	0.006	0.006	0.000	0.000	0.014	0.021	0.016	0.019
Al	0.202	0.199	0.199	0.206	0.205	0.196	0.201	0.143	0.211	0.162	0.167	0.145	0.138
Fe^{3+d}	0.004	0.004	0.005	0.004	0.004	0.003	0.003	0.003	0.000	0.009	0.010	0.009	0.010
Fe^{2+d}	0.038	0.037	0.039	0.032	0.033	0.027	0.026	0.000	0.000	0.084	0.085	0.078	0.060
Mn	0.000	0.001	0.001	0.001	0.001	0.001	0.001	0.000	0.000	0.002	0.000	0.000	0.000
Mg	0.036	0.037	0.038	0.038	0.038	0.037	0.050	0.001	0.000	0.042	0.113	0.144	0.125
Ca	0.057	0.060	0.057	0.059	0.068	0.083	0.057	0.005	0.000	0.071	0.081	0.108	0.141
Na	0.083	0.087	0.080	0.080	0.081	0.080	0.082	0.074	0.177	0.073	0.079	0.039	0.057
K	0.011	0.011	0.018	0.027	0.011	0.011	0.011	0.050	0.000	0.016	0.013	0.006	0.040
P	0.003	0.002	0.002	0.002	0.002	0.002	0.002	0.000	0.000	0.008	0.006	0.000	0.006
Compositional parameters													
Si + Al	0.762	0.754	0.755	0.752	0.757	0.750	0.762	0.867	0.823	0.681	0.592	0.601	0.543
NBO/T	0.29	0.30	0.30	0.31	0.30	0.31	0.29	0.15	0.21	0.40	0.60	0.60	0.74
Π[e]	−1.868	−1.677	−1.713	−1.583	−1.662	−1.376	−1.848	−3.681	−2.856	−0.706	0.704	0.706	2.252
ASI	0.97	0.91	0.94	0.92	0.90	0.76	0.97	1.07	1.20	0.71	0.66	0.56	0.37
ANK	2.16	2.02	2.03	1.94	2.24	2.16	2.16	1.16	1.20	1.84	1.82	3.25	1.42
Ionic Porosity (%)	48.55	48.52	48.54	48.43	48.46	48.47	48.49	49.58	49.24	48.13	47.58	47.02	46.88

[a] Sample preparation method. C. seal = cold seal vessel; ex. = extrapolated. The icelandite experiment was conducted at ~quartz-fayalite magnetite buffer (+0 +1.5).
[b] CO_2 solubility, recalculated where necessary to 1300°C and 1 GPa as described in the text.
[c] n/a = not applicable.
[d] Fe^{3+}/Fe^{2+} calculated following Kress and Carmichael (1988).
[e] Π calculated following Dixon (1997).

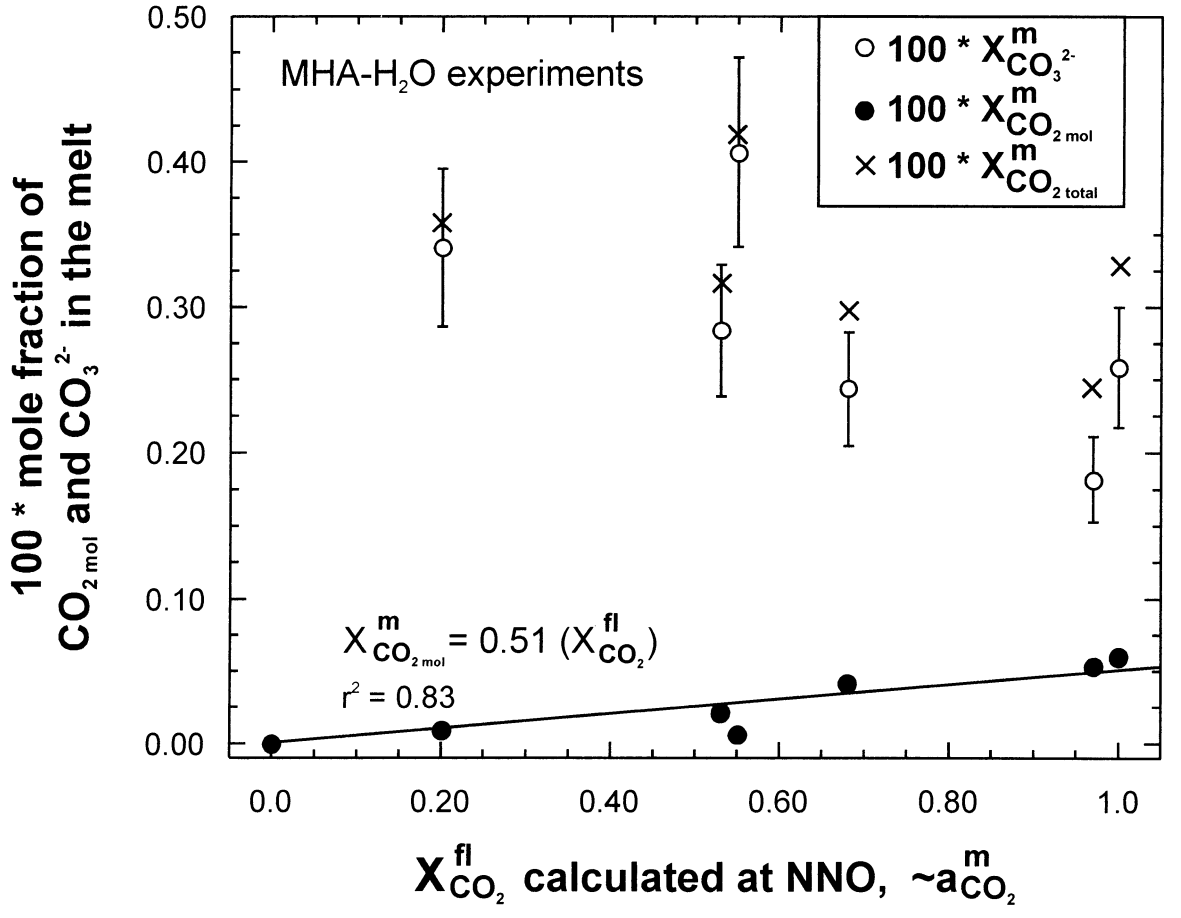

Fig. 3. Plot of $CO_{2\ total}$ solubility, CO_3^{2-} solubility, and $CO_{2\ mol}$ solubility expressed as mole fraction in the melt versus $X^{fl}_{CO_2}(\sim a^{melt}_{CO_2})$ for MHA-H_2O samples at NNO. Methods for determining mole fractions are described in the text. The $CO_{2\ total}$ and CO_3^{2-} solubility decrease with increasing $X^{fl}_{CO_2}(\sim a^{m}_{CO_2})$, indicating that Henry's law does not readily describe the relationship. The $CO_{2\ mol}$ solubility increases with increasing $X^{fl}_{CO_2}$, indicating that the behavior is Henrian.

One suggestion is that the changes in C-O speciation are related to different glass transition temperatures (Blank and Brooker 1994; Brooker et al. 1999). However, the dependence of the glass transition temperature on the H_2O_{total} content means that it is difficult to separate those two factors.

Another scenario is that the addition of H serves to depolymerize the melt and increase the abundance of O_r^{2-m} available to react with $CO^m_{2\ mol}$ to produce CO_3^{2-}. This idea is based on the observation that C-O speciation and carbonate peak splitting data change as a function of composition (polymerization; section 6.3). In the MHA-H_2O experiments, the abundance of O_r^{2-m} available could change via reactions of the type:

$$H_2O_{total} + \text{melt} \rightarrow H_2O^m_{mol} + O_r^{2-m} = 2OH^{-m} \quad (4)$$

(modified after Stolper, 1982). The overall general, unbalanced reaction could be:

$$CO^m_{2\ mol} + 2\text{T-}O_4^{2-m} + H_2O^m_{total} = CO_3^{2-m} + 2\text{T-}O_3^{-m} + 2OH^{-m} \quad (5)$$

where $\text{T-}O_4^{2-m}$ refers to nonbridging oxygens linked to T tetrahedra and $\text{T-}O_3^{-m}$ refers to bridging oxygens linked to T tetrahedra (Masson, 1965) that may be linked to CO_3^{2-}. The CO_3^{2-} could be coordinated by T in this reaction to form $(\text{2T-}O_3^- \ldots CO_3^{2-})^m$ such as Al- CO_3^{2-}-Al or Al- CO_3^{2-}-Si; however, if such species dominate the expected $\Delta\nu_3$ is 215 to 295 cm^{-1} (e.g., NaAlO-SiO_2 glasses; Fine and Stolper, 1985; Brooker et al., 1999), whereas values for andesite $\Delta\nu_3$ are $\sim$100 cm^{-1} (Table 1). In andesites, at least some of the CO_3^{2-} is likely bonded to M^{n+} ions such as Ca^{2+}, Mg^{2+}, or Fe^{2+} (Brooker et al., 2001b, see section 6.3).

Another possibility is that H interacts with the oxygens of the CO_3^{2-} groups, resulting in increased symmetry of the CO_3^{2-}. Hydrogen might form a bond(s) and/or a hydrogen bond(s) that modifies the charge or "effective" radius of the cation involved in bonding to the CO_3^{2-} oxygen(s). We refer to the resulting species as an X-CO_3^{2-}-X complex, where X = H_y, H_y-T, and H_y-M, and y refers to the number (0, 1 or 2) of H cations or hydrogen-bonded H. Some of the possible X-CO_3^{2-}-X species include H-Al-CO_3^{2-}-Si or H-M^{2+}-CO_3^{2-}-Al. Following this scheme a possible species is H_2CO_3, which would theoretically have a small $\Delta\nu_3$. However, we are reticent to suggest that it plays a major role because the $\Delta\nu_3$ for the H_2O-rich samples only differs from H_2O-poor samples by $\sim$10% relative. Unfor-

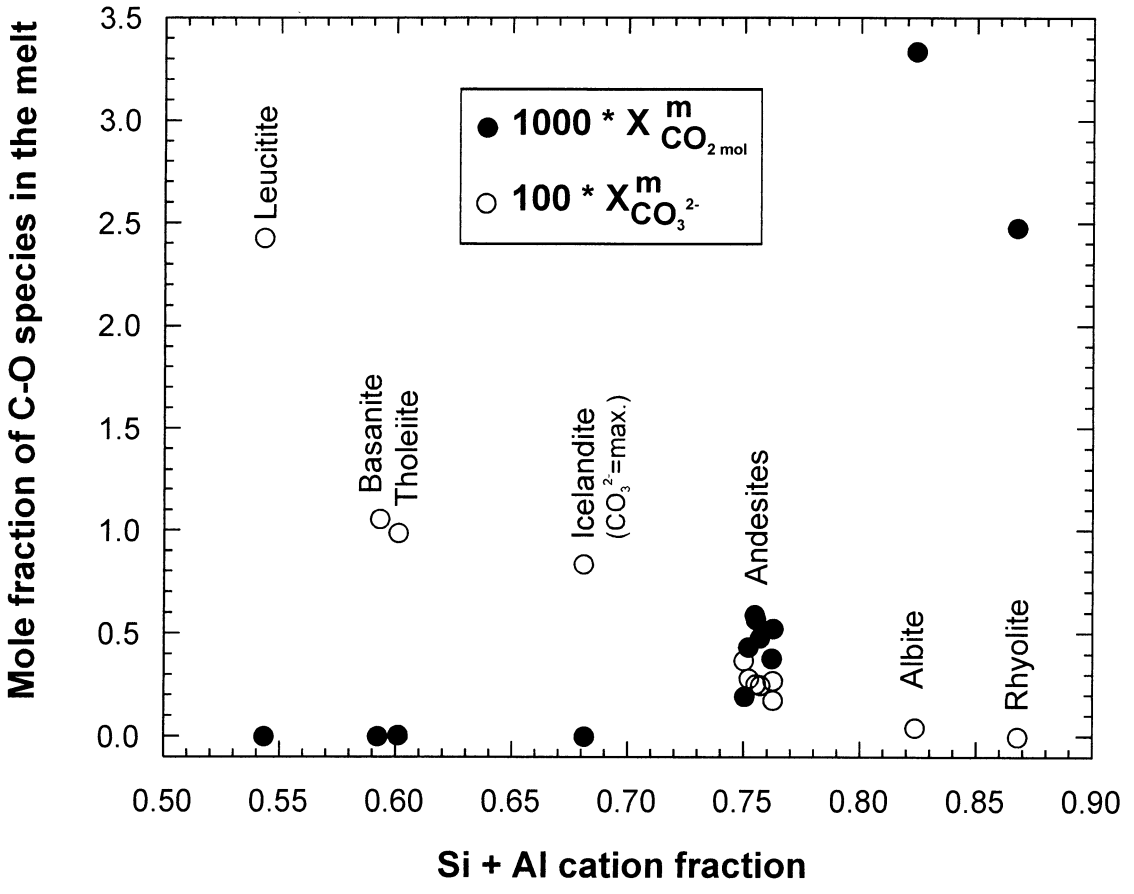

Fig. 4. C-O species solubility in mole fraction versus (Si + Al) mole fraction for the MHA-comp samples and samples from the literature (Table 3).

tunately, we have insufficient data to quantitatively evaluate the mole fraction of different X-CO_3^{2-}-X species, but we can write a general unbalanced reaction:

$$\text{cations} + CO_{2\,mol}^{m} + y/2\ H_2O_{total} = X\text{-}CO_3^{2-}\text{-}X \qquad (6)$$

where cations are T and M^{n+} cation(s).

6.3. Effect of Melt Composition on $CO_{2\ total}$ Solubility

To investigate $CO_{2\ total}$ solubility in a range of compositions, we examined literature data for rhyolite through leucitite, as well as the data for andesite (Tables 1 and 3). For the purposes of comparison, we assumed that the H_2O_{total} content was negligible in the literature samples. For basanite and rhyolite, the CO_2 solubility data were extrapolated from the literature data to the conditions of the experiments (1300°C and 1 GPa) using thermodynamic data determined for those specific compositions (Holloway and Blank, 1994). For tholeiitic basalt, $CO_{2\ total}$ solubility is 0.8 wt.% at 1300°C and 1 GPa (Pan et al., 1991). For albitic glass, we estimated the $CO_{2\ total}$ solubility (0.5 wt.%) and $CO_{2\ mol}$ and CO_3^{2-} contents based on Figure 7 in Stolper et al. (1987). For leucitite, a $CO_{2\ total}$ solubility of 2.85 wt.% was used (Thibault and Holloway, 1994). For icelandite, we used a CO_2 solubility value of 1.03 wt.%, which is a maximum value because the experiments had moderate H_2O_{total} contents and were at higher temperature (1400°C, 1 GPa; Jakobsson, 1997). The methods used for preparing the literature glasses and estimated f_{O_2} values are given in Table 3. We did not include some intermediate composition glasses in the study (Fine and Stolper, 1985; Brooker et al., 1999; Morizet et al., 2001) because the thermodynamic data necessary to extrapolate their $CO_{2\ total}$ solubilities to 1300°C and 1 GPa are unavailable or speciation data are unavailable.

6.3.1. Carbonate solubility

One of the goals of this study was to determine if CO_3^{2-} solubility is affected by varying the concentrations of T, H, or M^{n+} cations. The best predictor of CO_3^{2-} solubility for the compositional range examined was the mole fraction of (Si + Al) cations (Fig. 4 and Dixon et al., 1995). Carbonate increases for all samples as the mole fraction of (Si + Al) cations decreases and the melt becomes less polymerized (Fig. 4). Specific reactions of CO_3^{2-} with the T-O-T framework have been discussed by Taylor (1990).

Dixon (1997) developed a factor (Π) to predict CO_3^{2-} solubility in basalts. The Π factor includes (Si + Al) and M^{n+} cations ranked in order of decreasing Gibbs free energy of decarbonation (Ca > K > Na $\gg$ Mg $\sim$ Fe^{2+}; Spera and Bergman, 1980). The Π factor can be used to successfully

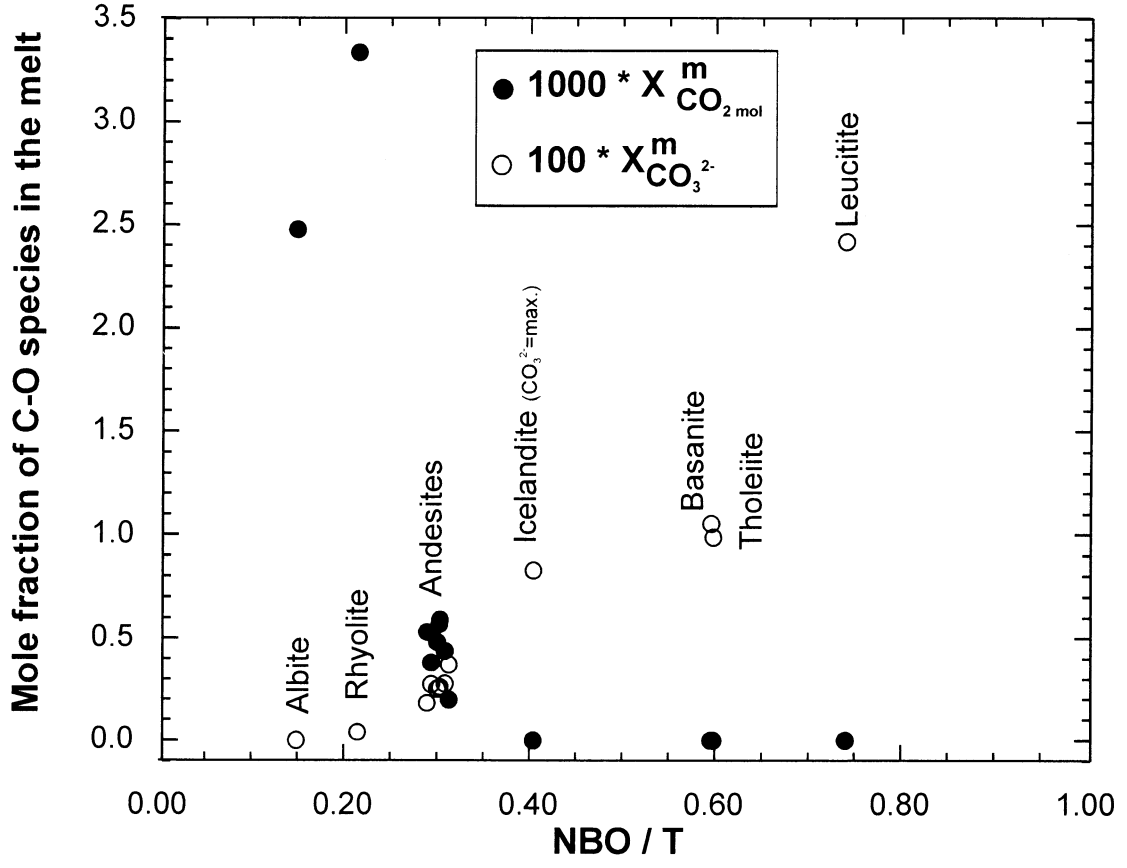

Fig. 5. C-O species solubility versus NBO/T for the MHA-comp samples and samples from the literature (Table 3).

predict $CO_{2\ total}$ solubility in basalts but, as noted by Dixon (1997), the linear trend cannot be extrapolated to compositions that contain $CO_{2\ mol}$ in addition to CO_3^{2-}, such as the andesites that we studied (Table 3).

Brooker et al. (2001a) developed an empirical third-order polynomial relationship between $CO_{2\ total}$ solubility and the ratio of non-binding oxygens (NBO) to tetrahedral components (T), where NBO = Mg + Ca + Na + K + Fe^{2+} and T = Si + Al + Fe^{3+} (Fig. 5, Eitel and Weyl, 1932; Mysen, 1976; Fine and Stolper, 1985; Brooker et al., 2001a). We observe a similar relationship in our dataset (Fig. 5). It is not clear whether this relationship is dominated by the cation fraction of T or the M^{n+} cations that make up non-bridging oxygens (NBO) (Table 3). The T cations make up the majority of the rock and therefore the NBO cations necessarily make up the remainder; however, to better understand the reaction mechanism it is necessary to examine the individual cations.

Within the andesite dataset, there is a general correlation between Ca and CO_3^{2-} concentrations (Table 3, Fig. 6). In addition, $\Delta\nu_3$ decreases as Ca content increases (Table 3), indicating that the CO_3^{2-} is more symmetrical, which may be more favorable for stabilizing CO_3^{2-} in the melt (Brey, 1976; Holloway et al., 1976). This relationship results either because the change in (Ca cation fraction(s) * Gibbs free energy of decarbonation) is greater than for any other cation (Spera and Bergman, 1980; Dixon, 1997) or because Ca has a high charge-to-radius ratio and is effective in breaking up the silicate network to produce O_r^{2-m} (Taylor, 1990).

Despite the general correlation between Ca and CO_3^{2-} observed in the MHA-comp data, this correlation is not observed in the range of compositions from rhyolite to leucitite (Table 3, Fig. 6). Furthermore, there is no clear relationship between CO_3^{2-} solubility and the Ca in the melt in excess of the normative feldspar component or aluminum saturation index (ASI) (Table 3). We suspect that the discrepancy between the MHA-comp data and the literature data is due to that fact that in the literature data Ca concentrations do not vary independently of the concentrations of other cations (e.g., T) and, therefore, in the literature compositions other cations might be more important in providing O_r^{2-m} to produce CO_3^{2-} in the melt.

Carbonate solubility shows a poor correlation with Mg in our experiments and the literature experiments (Table 3). This finding is in contrast to studies where the melts contained a larger mole fraction of Mg; in those cases, Mg may play a more important role (e.g., Ca-Mg-(Na)-Si-O compositions; Holloway et al., 1976; Brooker et al., 2001b). Based on our data (Table 3), we suggest that Fe^{2+} would behave in a similar manner to Mg, which is consistent with Gibbs Free energy of decarbonation.

For the MHA-comp andesite and literature samples, CO_3^{2-} solubility shows no overall correlation with K (Table 3). How-

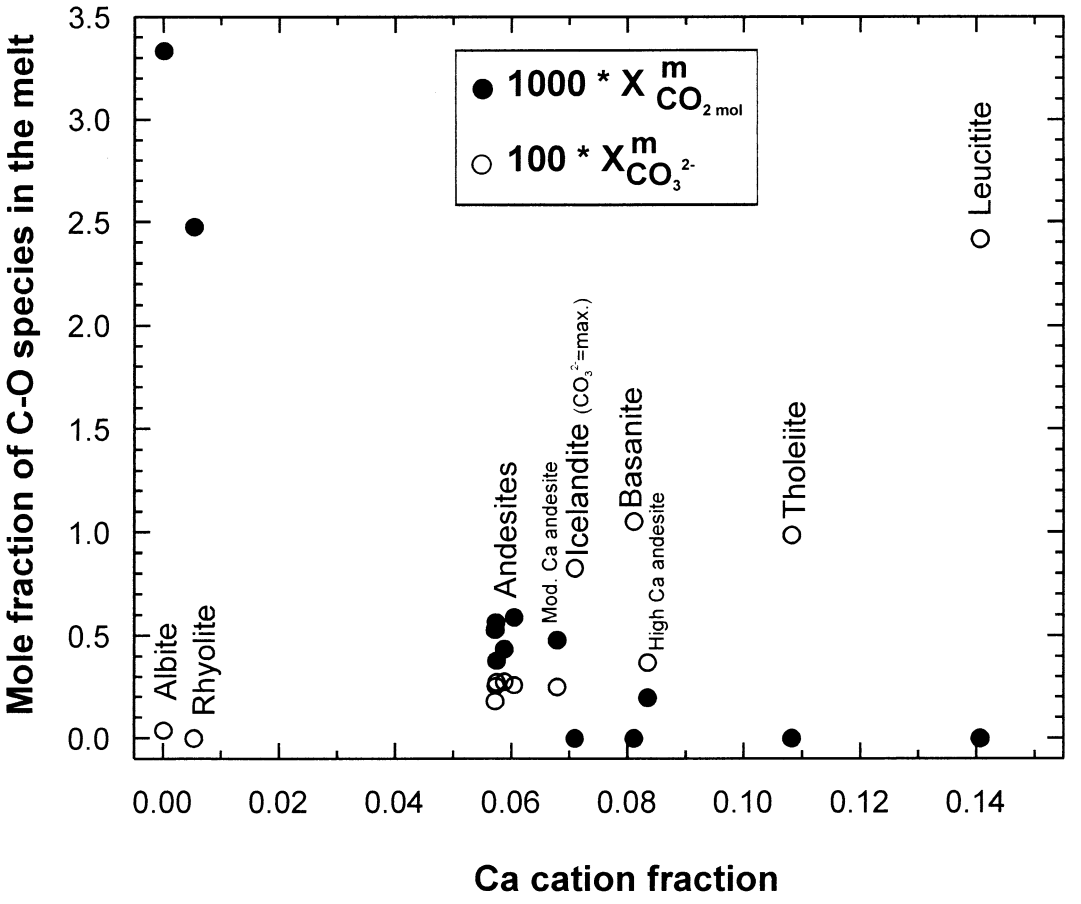

Fig. 6. C-O species solubility versus Ca mole fraction for the MHA-comp samples and samples from the literature (Table 3).

ever, the most K-rich sample, leucititic melt, contains the highest CO_3^{2-} solubility, possibly because it also has the lowest Si + Al. One might expect that K-rich magmas would contain higher CO_2 contents based on the abundance of CO_2 in K-rich rocks (kimberlites, leucitites, etc.), the low Si + Al of many K-rich rocks, and the high Gibbs free energy of decarbonation for K. In the samples we studied, it is possible that other cations (e.g., Ca) have a more dominant role in coordinating CO_3^{2-} in the melt. Perhaps CO_2 solubility is enhanced in natural K-rich melts because K is the major cation coordinating CO_3^{2-} anions.

6.3.2. Molecular CO_2 Solubility

The data set of compositions that contain $CO_{2\ mol}$ is limited, but the andesites add some compositional range. Compared to CO_3^{2-}, $CO_{2\ mol}$ has very weak trends with increasing (Si + Al) and Ca mole fractions. As the mole fraction of (Si + Al) increases, $CO_{2\ mol}$ increases somewhat (Fig. 4), and as Ca increases, $CO_{2\ mol}$ decreases somewhat (Fig. 6). Because CO_3^{2-} dominates in these glasses, the trends are more apparent when the fraction of $CO_{2\ mol}$ is examined relative to the mole fraction of total C-O species [$X_{CO_{2\ mol}}/(X_{CO_{2\ mol}} + X_{CO_3^{2-}})$; Table 3]. A negative correlation is observed between $CO_{2\ mol}$ and NBO/T (Table 3, Fig. 5), analogous to findings for $CO_{2\ total}$ contents (Brooker et al., 2001a) and noble gases (Shibata et al., 1998). Poor correlations are observed between $CO_{2\ mol}$ solubility and K, Mg, or Fe_{total} (Table 3).

6.4. Physical Properties of the Melt

Because we examined a range of compositions, our data can be used to study indirectly how $CO_{2\ total}$ solubility and speciation are affected by properties of the melt, such as ionic porosity (IP) and density. It is useful to investigate how those melt properties affect $CO_{2\ mol}$ solubility because reaction 2 shows that $CO_{2\ mol}$, unlike CO_3^{2-}, does not interact with the melt framework. In this way, $CO_{2\ mol}$ behaves in a similar manner to noble gases (Carroll and Stolper, 1993).

Noble gas solubility has been modeled as a function of ionic porosity (Carroll and Stolper, 1993), where:

$$IP = 100 * \{1 - (V_{ca}/V_m)\} \quad (7)$$

and V_{ca} is the molar volume calculated from ionic radii (Shannon and Prewitt, 1969) and V_m is the molar volume of the melt (at a specific temperature and pressure, following Lange and Carmichael, 1987). As ionic porosity increases, there are more "holes" available in the melt and the melt density decreases, therefore a larger concentration of a gas may dissolve.

The data show that $CO_{2\ mol}$ solubility has a positive correlation with IP (Fig. 7) and a negative correlation with melt

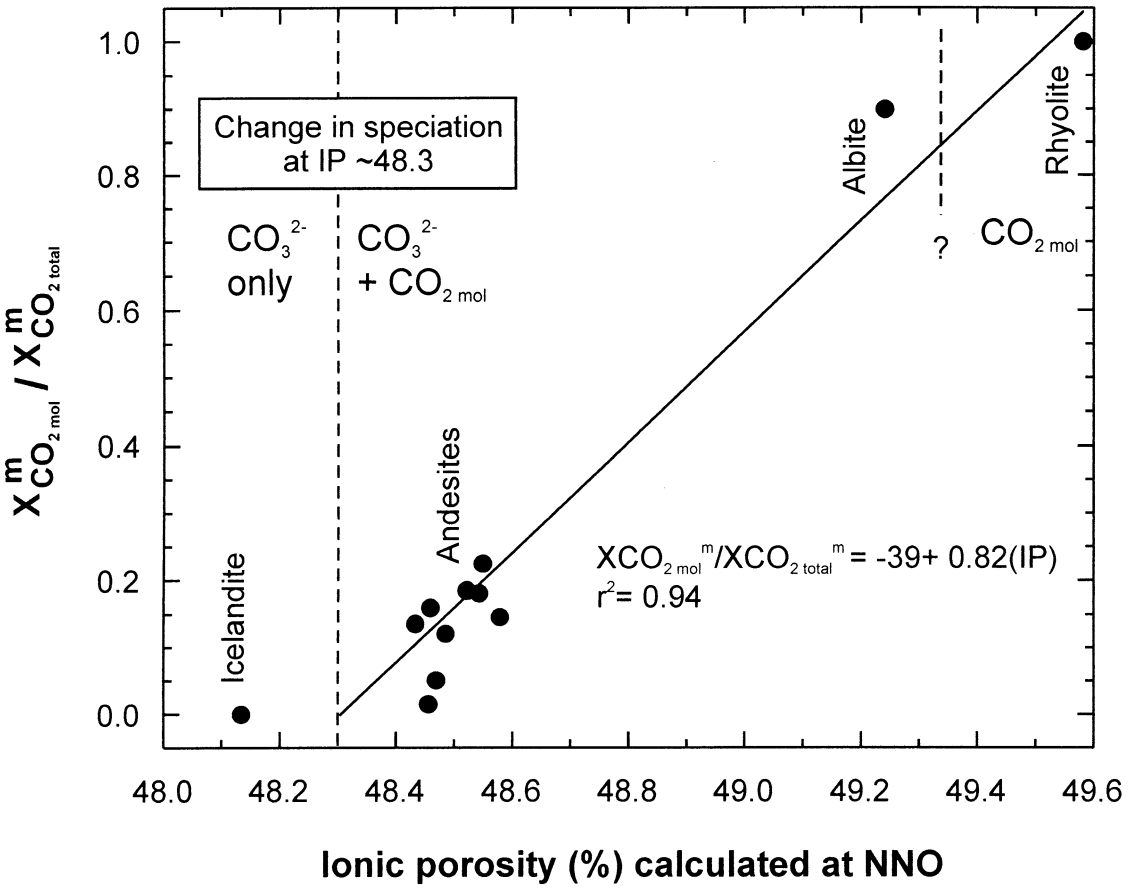

Fig. 7. $X^m_{CO_2\ mol}/X^m_{CO_2\ total}$ versus ionic porosity (IP) for the MHA-comp samples and samples from the literature (Table 3).

density (Table 3), as would be expected if $CO_{2\ mol}$ resides in "holes" in a melt. Thus, $CO_{2\ mol}$ is likely to be present in melts with ionic porosities greater than ~48% and absent in melts with lower ionic porosities. The regression curve indicates that it might be possible to predict $CO_{2\ mol}$ solubility in a melt based on ionic porosity; however, further data are necessary to test the validity of this approach.

6.5. $CO_{2\ total}$ Solubility Model

An integrated model for $CO_{2\ total}$ solubility in compositions with both $CO_{2\ mol}$ and CO_3^{2-} must account for the following observations:

1. $CO_{2\ total}$ solubility and speciation depend on melt composition: CO_3^{2-} solubility is highly correlated with the tetrahedral component (Si + Al fraction), and the NBO cation fraction(s) with the largest Gibbs free energy of decarbonation or the highest charge-to-radius ratio. In the intermediate compositions that we studied, Ca has the most important role. The solubility of $CO_{2\ mol}$ is dependent on physical properties that affect $CO_{2\ mol}$ dissolution in the melt, such as IP (or NBO/T).
2. $CO_{2\ total}$ solubility and speciation depend on H_2O content: as H_2O_{total} increases, CO_3^{2-} increases and $CO_{2\ mol}$ decreases, although these changes are not related to H-O speciation.

Below, we combine those observations to propose a general model for $CO_{2\ total}$ solubility in melts.

Reaction 3, involving CO_3^{2-}, is dependent on both the available free oxygen (O_r^{2-m}) and on the availability of M^{n+} cations that react with $CO_{2\ mol}$ (Spera and Bergman, 1980; Holloway, 1981; Fine and Stolper, 1985). Adapting those authors' approach, but writing the reaction to include H (reaction 6) we can write a general unbalanced reaction:

$$CO^m_{2\,mol} + \text{cations (T and } M^{n+}) + O_r^{2-m} + \frac{y}{2} H_2O_{total} \Rightarrow X - CO_3^{2-} - X \quad (8)$$

Until we can measure the amount of M, T, and H coordinating with CO_3^{2-} in silicate glasses, we will not be able to determine the stoichiometry for reaction 8 or the potential interdependence of the cations.

As indicated above, both $CO_{2\ mol}$ and CO_3^{2-} contents are dependent, to some degree, on melt polymerization. For H_2O-poor samples, the transition from $CO_{2\ mol}$-bearing samples to

$CO_{2\ mol}$-free samples appears to occur between icelandite and andesite at a NBO/T of ~0.3 (Fig. 5). For $CO_{2\ mol}$, IP likely has a role and the transition between samples dominated by CO_3^{2-} and those dominated by $CO_{2\ mol}$ occurs at ~48.3% (Fig. 7).

7. CONCLUSIONS

We conducted experiments on $CO_{2\ total}$ solubility in andesitic melts as a function of H_2O_{total} content and melt composition:

1. In intermediate compositions, CO_3^{2-} is the dominant C-O species, with minor molecular $CO_{2\ mol}$. C-O speciation and solubility are both dependent on H_2O_{total}. At 1300°C and 1 GPa, the effect of H_2O_{total} on $CO_{2\ total}$ solubility is to increase $CO_{2\ total}$ wt.% by ~0.06 wt.% per wt.% of H_2O_{total}.
2. $CO_{2\ total}$ solubility, which is dominated by CO_3^{2-}, is enhanced at lower mole fraction of (Si + Al). Carbonate solubility is also correlated with M^{n+} cations with large Gibbs free energy of decarbonation or high charge-to-radius ratio cations because these cations interact with the silicate network and enhance the formation of CO_3^{2-}. In intermediate melts, Ca has an important role in controlling the bonding environment and solubility of CO_3^{2-}.
3. A two-stage model for $CO_{2\ total}$ solubility is proposed. First, CO_2 is dissolved as $CO_{2\ mol}$ in the melt as a function of $X^{fl}_{CO_2}$, which approximates $a^{m}_{CO_2}$. Higher $CO_{2\ mol}$ solubility is found in compositions with high IP and high polymerization or low H_2O_{total} content and lower NBO. Second, $CO_{2\ mol}$ reacts with the O_r^{2-m} to form CO_3^{2-}. The cations attached to the oxygens in the CO_3^{2-} include T, M^{n+}, H_y, H_y-T, and H_y-M. Carbonate is the dominant C-O species in many silicate melts, and is favored in melts that are depolymerized with relatively high M^{n+} cation fractions and H_2O contents, and with NBO/T less than 0.3.
4. The results of this study provide constraints to better determine what factors affect $CO_{2\ total}$ solubility in silicate melts. The data indicate that because H_2O enhances $CO_{2\ total}$ solubility, the quantity of $CO_{2\ total}$ dissolved in the melt, at a given pressure, will be higher. Thus, bubble nucleation would occur at shallower levels and fluid production (Δmass of $CO_2/\Delta P$, at constant temperature and composition) will be greater. If this is true, then the effects of H_2O on CO_2 need to be incorporated into solubility models (Papale, 1999), degassing models, and the models for the formation of hydrothermal ore deposits.

Acknowledgments—We thank the following people for helpful discussions: J. Dixon, A. Grzechnik, S. Jakobsson, J. Lowenstern, G. Moore, D. Vielzeuf, H. W. Nesbitt, H. D. Zimmerman, and K. Roggensack. M. Carroll and S. Newman provided computer programs for density calculations. D. Eggler provided the Mt. Hood andesite composition powder. J. Forneris prepared samples Juli9 and Juli12. The USGS Menlo Park is thanked for access to their FTIR. We thank B. R. Frost, F. Spera, and two anonymous reviewers for their suggestions. This work was supported by NSF grants EAR-9506494 and EAR-9973066 (Holloway), EAR-9614325 (Hervig and Holloway), and EAR-9614229 (McMillan).

Associate editor: B. R. Frost

REFERENCES

Blank J. G. and Brooker R. A. (1994) Experimental studies of carbon dioxide in silicate melts: Solubility, speciation, and stable carbon isotope behavior. In *Volatiles in Magmas* (eds. M. R. Carroll and J. R. Holloway), Vol. 30, pp. 157–186. Mineral. Soc. Am., Washington, DC.

Blank J. G., Stolper E. M., and Carroll M. R. (1993) Solubilities of carbon dioxide and water in rhyolitic melt at 850°C and 750 bars. *Earth Planet. Sci. Lett.* **119,** 27–36.

Brey G. (1976) CO_2 solubility and solubility mechanisms in silicate melts at high pressures. *Contrib. Mineral. Petrol.* **57,** 215–221.

Brooker R., Holloway J. R., and Hervig R. L. (1998) Reduction in piston-cylinder experiments: The detection of carbon infiltration into platinum capsules. *Am. Mineral.* **83,** 985–994.

Brooker R. A., Kohn S. C., Holloway J. R., and McMillan P. F. (2001a). Structural controls on the solubility of CO_2 in silicate melts. Part I: bulk solubility data. *Chem. Geol.* **174,** 225–239.

Brooker R. A., Kohn S. C., Holloway J. R., and McMillan P. F. (2001b). Structural controls on the solubility of CO_2 in silicate melts. Part II: IR characteristics of carbonate groups in silicate glasses. *Chem. Geol.* **174,** 241–254.

Brooker R. A., Kohn S. C., Holloway J. R., McMillan P. F., and Carroll M. R. (1999) Solubility, speciation and dissolution mechanisms of CO_2 in melts along the $NaAlO_2$-SiO_2 join. *Geochim. Cosmochim. Acta* **63,** 3549–3565.

Burnham C. W. (1979) The importance of volatile constituents. In *The Evolution of the Igneous Rocks: Fiftieth Anniversary Perspectives* (ed. H. S. Yoder Jr.), pp. 439–482. Princeton University Press.

Carroll M. R. and Stolper E. M. (1993) Noble gas solubilities in silicate melts and glasses: New experimental results for argon and the relationship between solubility and ionic porosity. *Geochim. Cosmochim. Acta* **57,** 5039–5051.

Dixon J. E. (1997) Degassing of alkalic basalts. *Am. Mineral.* **82,** 368–378.

Dixon J. E. and Pan V. (1995) Determination of the molar absorptivity of dissolved carbonate in basanitic glass. *Am. Mineral.* **80,** 1339–1342.

Dixon J. E., Stolper E. M., and Holloway J. R. (1995) An experimental study of water and carbon dioxide solubilities in mid-ocean ridge basaltic liquids. Part I: Calibration and solubility models. *J. Petrol.* **36,** 1607–1631.

Eggler D. H. and Kadik A. A. (1979) The system $NaAlSi_3O_8$-H_2O-CO_2 to 20 kbar pressure: I. Compositional and thermodynamic relations of liquids and vapors coexisting with albite. *Am. Miner.* **64,** 1036–1048.

Eggler D. H. and Rosenhauer M. (1978) Carbon dioxide in silicate melts: II. Solubilities of CO_2 and H_2O in $CaMgSi_2O_8$ (diopside) liquids and vapors at pressures to 40 kb. *Am. J. Sci.* **278,** 64–94.

Eitel W. and Weyl W. (1932) Residuals in the melting of commercial glasses. *J. Am. Cer. Soc.* **15,** 159–166.

Fine G. J. and Stolper E. M. (1985) The speciation of carbon dioxide in sodium aluminosilicate glasses. *Contrib. Mineral. Petrol.* **91,** 105–121.

Frost D. J. and Wood B. J. (1995) Experimental measurements of the graphite C-O equilibrium and CO_2 fugacities at high temperature and pressure. *Contrib. Mineral. Petrol.* **121,** 303–308.

Gill J. B. (1981) *Orogenic Andesites and Plate Tectonics*. Springer.

Holloway J. R. (1981) Volatile interactions in magmas. In *Thermodynamics of Minerals and Melts*, Vol. 1 (eds. R. C. Newton, A. Navrotsky, and B. J. Wood), pp. 273–293. Springer-Verlag.

Holloway J. R. and Blank J. G. (1994) Application of experimental results to C-O-H species in natural melts. In *Volatiles in Magmas*, Vol. 30 (eds. M. R. Carroll and J. R. Holloway), pp. 187–230. Mineral. Soc. Am., Washington, DC.

Holloway J. R., Burnham C. W., and Millhollen G. L. (1968) Generation of H_2O-CO_2 mixtures for use in hydrothermal experimentation. *J. Geophys. Res.* **73,** 6598–6600.

Holloway J. R. and Lewis C. F. (1974) CO_2 solubility in hydrous albite liquid at 5 kbar. *EOS, Trans. Am. Geophys. Union.* **55,** 483.

Holloway J. R., Mysen B. O., and Eggler D. H. (1976) The solubility of CO_2 in liquids on the join CaO-MgO-SiO_2-CO_2. *Carn. Inst. Wash. Yr. Bk.* **1700,** 626–630.

Jakobsson S. (1997) Solubility of water and carbon dioxide in an icelandite at 1400°C and 10 kilobars. *Contrib. Mineral. Petrol.* **127,** 129–135.

Jendrzejewski N., Trull T. W., Pineau F., and Javoy M. (1997) Carbon solubility in Mid-Ocean Ridge basaltic melt at low pressures (250–1950 bar). *Chem. Geol.* **138,** 81–92.

Kawamoto T. and Hirose K. (1994) Au-Pd sample containers for melting experiments on iron and water bearing systems. *Eur. J. Mineral.* **6,** 381–385.

King P. L. (1999) C-O-H Volatiles in igneous rocks: Experimental and natural studies of hydrous minerals (amphiboles) and glasses (melts). Ph.D. dissertation, Arizona State University.

King P. L., Holloway J. R., Hervig R. L., Delaney J. S., and Dyar M. D. (2000) Partitioning of H and Fe^{3+}/Fe_{total} between amphibole and basaltic melt as a function of oxygen fugacity. *Earth Planet. Sci. Lett.* **178,** 97–112.

King P. L., Vennemann T., Holloway J. R., Hervig R. L., Lowenstern J., and Forneris J. (2002). Analytical techniques for volatiles: A case study using intermediate (andesitic) glasses. *Am. Mineral.* (submitted).

Kress V. C. and Carmichael I. S. E. (1988) Stoichiometry of the iron oxidation reaction in silicate melts. *Am. Mineral.* **73,** 1267–1274.

Lange R. A. and Carmichael I. S. E. (1987) Densities of Na_2O-K_2O-CaO-MgO-FeO-Fe_2O_3-Al_2O_3-TiO_2-SiO_2 liquids: New measurements and derived partial molar properties. *Geochim. Cosmochim. Acta* **51,** 2931–2946.

Luth W. C., Jahns R. H., and Tuttle O. F. (1964) The granite system at pressures of 4 to 10 kilobars. *J. Geophys. Res.* **69,** 759–773.

Mandeville C. W., Webster J. D., Rutherford M. J., Taylor B. E., Timbal A., and Faure K. (2001). Determination of extinction coefficients for infrared absorption bands of H_2O in andesitic glasses. *Am. Mineral.* in revision.

Masson C. R. (1965) An approach to the problem of ionic distribution in liquid silicates. *Proc. Roy. Soc. Lond.* **A287**, 201–221.

Morizet Y., Brooker R. A., and Kohn S. C. (2001) CO_2 in haplophonolite melt: Solubility, speciation and carbonate complexation. *Geochim. Cosmochim. Acta* (in press).

Mysen B. O. (1976) The role of volatiles in silicate melts: Solubility of carbon dioxide and water in feldspar, pyroxene, and feldspathoid melts to 30 kb and 1625°C. *Am. J. Sci.* **276,** 969–996.

Mysen B. O., Arculus R. J., and Eggler D. H. (1975) Solubility of carbon dioxide in melts of andesite, tholeiite, and olivine nephelinite composition to 30 kbar pressure. *Contrib. Mineral. Petrol.* **53,** 227–239.

Mysen B. O., Eggler D. H., Seitz M. G., and Holloway J. R. (1976) Carbon dioxide in silicate melts and crystals. Part I. Solubility measurements. *Am. J. Sci.* **276,** 455–479.

Nowack M. and Behrens H. (2001). Water in rhyolitic magmas: Getting a grip on a slippery problem. *Earth Planet. Sci. Lett.* **184,** 515–522.

Pan V., Holloway J. R., and Hervig R. L. (1991) The pressure and temperature dependence of carbon dioxide solubility in tholeiitic basalt melts. *Geochim. Cosmochim. Acta* **55,** 1587–1595.

Papale P. (1999) Modeling of the solubility of a two-component H_2O + CO_2 fluid in silicate liquids. *Am. Mineral.* **84,** 477–492.

Pawley A. R., Holloway J. R., and McMillian P. F. (1992) The effect of oxygen fugacity on the solubility of carbon-oxygen fluids in basaltic melt. *Earth Planet. Sci. Lett.* **110,** 213–225.

Saxena S. K. and Fei Y. (1987) High pressure and high temperature fluid fugacities. *Geochim. Cosmochim. Acta* **51,** 783–791.

Shannon R. D. and Prewitt C. T. (1969) Effective ionic radii in oxides and fluorides. *Acta Crysta.* **B25,** 925–946.

Shibata T., Takahashi E., and Matsuda J.-I. (1998) Solubility of neon, argon, krypton, and xenon in binary and ternary silicate systems: A new view on noble gas solubility. *Geochim. Cosmochim. Acta* **62,** 1241–1253.

Shilobreyeva S. N. and Kadik A. A. (1990) Solubility of CO_2 in magmatic melts at high temperatures and pressures. *Geochem. Int.* **27,** 31–41.

Spera F. J. and Bergman S. C. (1980) Carbon dioxide in igneous petrogenesis: I. Aspects of the dissolution of CO_2 in silicate liquids. *Contrib. Mineral. Petrol.* **74,** 55–66.

Stolper E., Fine G., Johnson T., and Newman S. (1987) Solubility of carbon dioxide in albitic melt. *Am. Mineral.* **72,** 1071–1085.

Stolper E. M. (1982) The speciation of water in silicate melts. *Geochim. Cosmochim. Acta* **46,** 2609–2620.

Symonds R. B., Rose W. I., Bluth G. J. S., and Gerlach T. M. (1994) Volcanic-gas studies: Methods, results, and applications. In *Volatiles in Magmas*, Vol. 30 (eds. M. R. Carroll and J. R. Holloway), pp. 1–66. Mineral. Soc. Am., Washington, DC.

Tamic N., Behrens H., and Holtz F. (2001). The solubility of H_2O and CO_2 in rhyolitic melts in equilibrium with a mixed CO_2-H_2O fluid phase. *Chem. Geol.* **174,** 333–347.

Taylor W. R. (1990) The dissolution mechanism of CO_2 in aluminosilicate melts: Infrared spectroscopic constraints on the cationic environment of dissolved $[CO_3]^{2-}$. *Eur. J. Mineral.* **2,** 547–563.

Thibault Y. and Holloway J. R. (1994) Solubility of CO_2 in a Ca-rich leucitite: Effects of pressure, temperature, and oxygen fugacity. *Contrib. Mineral. Petrol.* **116,** 216–224.

Tingle T. N. and Aines R. D. (1988) Beta trace autoradiography and infrared spectroscopy bearing on the solubility of CO_2 in albite melt at 2 GPa and 1450°C. *Contrib. Mineral. Petrol.* **100,** 222–225.

Withers A. C., Zhang Y. X., and Behrens H. (1999) Reconciliation of experimental results on H_2O speciation in rhyolitic glass using in-situ and quenching techniques. *Earth Planet. Sci. Lett.* **173,** 343–349.